A&A 595, A74 (2016)
DOI: 10.1051/0004-6361/201628999

Astronomy & Astrophysics

HDO and SO_2 thermal mapping on Venus

III. Short-term and long-term variations between 2012 and 2016

T. Encrenaz[1], T. K. Greathouse[2], M. J. Richter[3], C. DeWitt[3], T. Widemann[1,4], B. Bézard[1], T. Fouchet[1], S. K. Atreya[5], and H. Sagawa[6]

[1] LESIA, Observatoire de Paris, CNRS, PSL University, UPMC, UPD, 92195 Meudon, France
e-mail: therese.encrenaz@obspm.fr
[2] SWRI, Div. 15, San Antonio, TX 78228, USA
[3] Physics Department, University of California, Davis CA 95616, USA
[4] Université Versailles St-Quentin, DYPAC EA 2449, 78280 Guyancourt, France
[5] Department of Atmospheric, Oceanic and Space Science, University of Michigan, Ann Arbor, MI 48109-2143, USA
[6] Faculty of Science, Kyoto-Sangyo University, Motoyama, Kamigamo, Kita-ku, 603-8555 Kyoto, Japan

Received 25 May 2016 / Accepted 2 August 2016

ABSTRACT

We present the analysis of a four-year observational campaign using the TEXES high-resolution imaging spectrometer at the NASA Infrared Telescope Facility to map sulfur dioxide and deuterated water over the disk of Venus. Data have been recorded in two spectral ranges around 1345 cm^{-1} (7.4 μm) and 530 cm^{-1} (19 μm) in order to probe the cloudtop at an altitude of about 64 km (SO_2 and HDO at 7.4 μm) and a few kilometers below (SO_2 at 19 μm). Observations took place during six runs between January 2012 and January 2016. The diameter of Venus ranged between 12 and 33 arcsec. Data were recorded with a spectral resolving power up to 80 000 and a spatial resolution of about 1 arcsec (at 7.4 μm) and 2.5 arcsec (at 19 μm). Mixing ratios were estimated from HDO/CO_2 and SO_2/CO_2 line depth ratios, using weak neighboring transitions of comparable depths. The whole dataset demonstrates that the two molecules behave very differently to each other. The HDO maps are uniform over the disk. The disk-integrated H_2O mixing ratio (estimated assuming a D/H of 200 VSMOW in the mesosphere of Venus) show moderate variations (by less than a factor of 2) over the four-year period. A value of 1.0−1.5 ppmv is obtained in most of the cases. The SO_2 maps, in contrast, show strong variations over the disk of Venus, by a factor as high as 5. Long-term variations of SO_2 show that the disk-integrated SO_2 mixing ratio also varies between 2012 and 2016 by a factor as high as ten, with a minimum value of 30 +/−5 ppbv on February 26, 2014 an a maximum value of 300 +/−50 ppbv on January 14, 2016. The SO_2 maps also show a strong short-term variability. It can be seen that the SO_2 maximum feature usually follows the four-day rotation of the clouds over a timescale of two hours, which corresponds to a rotation of 7.5 deg over the planetary disk, but its morphology also changes, which suggests that the lifetime of this structure is not more than a few hours.

Key words. techniques: imaging spectroscopy – planets and satellites: atmospheres – planets and satellites: terrestrial planets – planets and satellites: composition

1. Introduction

The atmospheric chemistry of Venus is known to be driven by two species, water vapor and sulfur dioxide (Krasnopolsky 1986, 2010). Both are present in the lower troposphere with mixing ratios of about 30 and 100 ppmv respectively, and, at low latitude, are carried upward by Hadley convection. SO_2 is photodissociated and forms SO_3 which combines with water to form sulfuric acid. H_2SO_4 condenses above an altitude of 40 km to form the major constituent of the cloud deck. Above the top of this cloud, at about 65−70 km, H_2SO_4 is dissociated by the solar UV radiation to form H_2O and SO_3, then SO_2, SO and possible other sulfur species. The abundances of H_2O and SO_2 above the clouds are in the range of 1−2 ppmv (Fedorova et al. 2008; Belyaev et al. 2008) and 10−100 ppbv (Zasova et al. 1993; Marcq et al. 2013) respectively. Higher in the mesosphere, at an altitude of 80−100 km, there is evidence for an increase in the SO_2 abundance, probably fed by a second sulfur reservoir (Sandor et al. 2010, 2012).

Despite extended ground-based and space observing campaigns, the photochemistry and dynamics of the Venus mesosphere is far from being understood. UV and infrared data recorded by VMC, SPICAV, SPICAV/SOIR and VIRTIS aboard Venus Express show evidence for drastic variations in the mesospheric temperature and CO_2 profiles, the wind distribution at the cloud level, and the abundance of SO_2 above the clouds (Vandaele et al. 2016). Submillimeter observations of SO and SO_2 in the upper mesosphere show evidence for large variations in the abundances of these species (especially SO) on timescales as short as a day (Sandor et al. 2012). In addition, the long-term variation of the SO_2 abundance identified by Esposito (1984) over a timescale of several years, using the Ultra-Violet Spectrometer (UVS) aboard Pioneer Venus orbiter, and later observed by Venus Express (Marcq et al. 2013) is still not understood.

Orbiter space observations usually observe a small part of the planet with high spatial resolution at a fixed local time. Ground-based imaging spectroscopy in the thermal infrared range provides another complementary means, as it allows the simultaneous mapping of the Venus disk in a short time. It is thus best

suited for studying day vs. night effects (near quadrature) or morning vs. evening effects (near superior conjunction).

Since January 2012, we have been monitoring the abundances of SO_2 and HDO above and within the clouds, by using high-resolution infrared spectroscopy in the thermal regime at different wavelengths. In 2012, we used the Texas Echelon Multi Echelle Spectrograph (TEXES) at the Infrared Telescope Facility (IRTF) at 7.4 μm (probing the cloudtop) and at 19 μm (probing within the cloud a few kilometers i.e., about one scale height) below. These data have shown that SO_2 and HDO behave very differently. HDO (used as a tracer for H_2O) shows moderate spatial and temporal variations, while SO_2, in contrast, exhibits strong local variations over the disk and strong temporal variations with timescales ranging from hours to months. In addition, the 2012 data show evidence for a depletion of SO_2 a few kilometers above the cloudtop, while the HDO mixing ratio appears to be more or less constant in the mesosphere (Encrenaz et al. 2012, 2013, hereafter referred as E12 and E13).

Our observing campaign with TEXES was carried out with four additional runs, in February 2014, July 2014, March 2015 and January 2016. Data were obtained at 7.4 μm (study of SO_2 and HDO at the cloudtop), 19 μm (study of SO_2 within the cloud), and in two bands of CO_2 at 10.5 and 12.9 μm to retrieve information on the mesospheric temperature distribution. The study of the thermal structure and its variability will be presented in a forthcoming publication. In this paper we present the study of the SO_2 and HDO abundances and their variability, using the results of the six datasets. Observations and modeling are described in Sect. 2. Results are presented in Sect. 3 and discussed in Sect. 4. Conclusions are summarized in Sect. 5.

2. Observations and modeling

2.1. Observations

TEXES is an infrared imaging spectrometer operating between 5 and 25 μm, which combines high spatial (about 1 arcsec) and spectral (R = 80 000 at 7.4 μm, R = 70 000 at 19 μm) resolution (Lacy et al. 2002). Since 2001, we have been mapping the Martian disk with the TEXES instrument at the IRTF, with the principal objective of detecting and mapping hydrogen peroxide, and monitoring its seasonal variations. In addition, we used weak transitions of HDO to monitor the water vapor simultaneously (Encrenaz et al. 2005, 2008, 2012, 2015a). To retrieve the maps of the H_2O_2 and HDO mixing ratios, we selected weak transitions of these species and calculated the ratio of their line depth versus the line depth of a neighboring weak CO_2 line. As discussed by Encrenaz et al. (2015a), this method has the advantage of minimizing the uncertainties associated with the atmospheric parameters (temperature profile) and geometrical effects (airmass).

Since January 2012, we have been continuing to apply the same method to monitor the SO_2 and HDO content at the cloudtop of Venus. As discussed by Zasova et al. (1993) from the Venera-15 orbiter data, observations in the thermal infrared (between 6 and 20 μm) allow us to probe different atmospheric levels. Outside the strong ν_2 band of CO_2 centered at 15 μm (660 cm^{-1}), the penetration level depends upon the H_2SO_4 extinction cross section which shows a maximum around 1200 cm^{-1} (8.3 μm, Zasova et al. 1993). The SO_2 molecule shows three ro-vibrational bands in this range. The strongest band (ν_3) lies around 1350 cm^{-1} (7.3 μm) and the corresponding penetration level is near the cloudtop. We have selected the 1343–1351 cm^{-1} range which contains, in addition to numerous SO_2 transitions, a few HDO lines. An isotopic band of CO_2 is also present, including strong and weak CO_2 transitions.

The second SO_2 band (ν_2), at 530 cm^{-1} (19 μm) is about eight times weaker than the ν_3 band (Pugh & Rao 1976), but its penetration level is a few kilometers (i.e., about one scale height) below, because the H_2SO_4 extinction coefficient at this wavelength is about three times weaker than at 1350 cm^{-1}. We have selected the 529–531 cm^{-1} interval which contains several SO_2 and CO_2 weak transitions with, in addition, a strong CO_2 line. A third SO_2 band (ν_1), with an integrated strength comparable to the one of the ν_2 band (Pugh & Rao 1976) is centered around 1150 cm^{-1} and probes higher levels, as the corresponding H_2SO_4 extinction coefficient is three times stronger than at 7.4 μm. The 1155–1160 cm^{-1} interval also contains some weak SO transitions but these lines were not detected in the TEXES data. The detection of the SO_2 ν_1 band is also difficult since, as shown in our previous study (E13), the SO_2 mixing ratio is depleted above the clouds. The band was detected by Zasova et al. (1993), in an epoch corresponding to a high SO_2 content. We tried to detect the band in February 2014 but were unable to identify it. This is consistent with our expectations, since, as explained below, the SO_2 content was especially low at that date. In addition, we observed two CO_2 bands, at 792 cm^{-1} (12.6 μm) and 955 cm^{-1} (10.5 μm), with the purpose of retrieving the thermal structure of the mesosphere. A first analysis of these data has been published in E13. In the present paper, we concentrate our analysis on the abundance of SO_2 (retrieved from the ν_3 and ν_2 bands of SO_2, at 7.4 and 19 μm respectively) and on the abundance of H_2O (retrieved from the HDO band at 7.4 μm). Some results of our previous analyses have been reconsidered, using an updated conversion of the pressure and altitude scales. In order to convert the HDO mixing ratio into a H_2O mixing ratio, we have assumed, in the mesosphere of Venus, a D/H ratio of 200 times the standard terrestrial value (VSMOW). This value, also used by Krasnopolsky (2010), was chosen following Bertaux et al. (2007) and Fedorova et al. (2008).

The principle of our analysis is described in the following. From the map of the continuum flux, at 7.4 and 19 μm (measured between the terrestrial and planetary absorption lines), we can infer the temperatures of the penetration levels at these two wavelengths. Using a nominal thermal model at low latitude as a first guess, we can derive the pressures of these levels, and an information about their altitudes. To model our synthetic spectra we used only the pressure, and not the altitude; we have no information about the atmosphere below the penetration levels. Using the line depth of a weak CO_2 line, we can get information on the thermal gradient above the penetration level; the measurement at both 7.4 and 19 μm allows to check the consistency of the retrieved thermal profile (E13). By making the ratio of a weak SO_2 line depth with respect to a weak neighboring line of CO_2, we infer a map of the SO_2 mixing ratio, both at 7.4 and 19 μm; a map of the HDO mixing ratio is obtained at 7.4 μm from the ratio of two HDO and CO_2 weak transitions. By using simultaneously weak and strong transitions, at 7.4 and 19 μm, as well as in the dedicated CO_2 observations at 10.5 and 12.6 μm, we can get information about the mesospheric thermal structure and its variation with the local time. In addition, the spectral fitting of disk-integrated spectra at 7 and 19 μm gives us information about the vertical distribution of SO_2 and HDO. Finally, repeated observations at different timescales (from hours to years) gives un insight on the short-term and long-term variability of these species.

Table 1 lists the main characteristics of our observing runs between January 2012 and January 2016, and Fig. 1 shows the

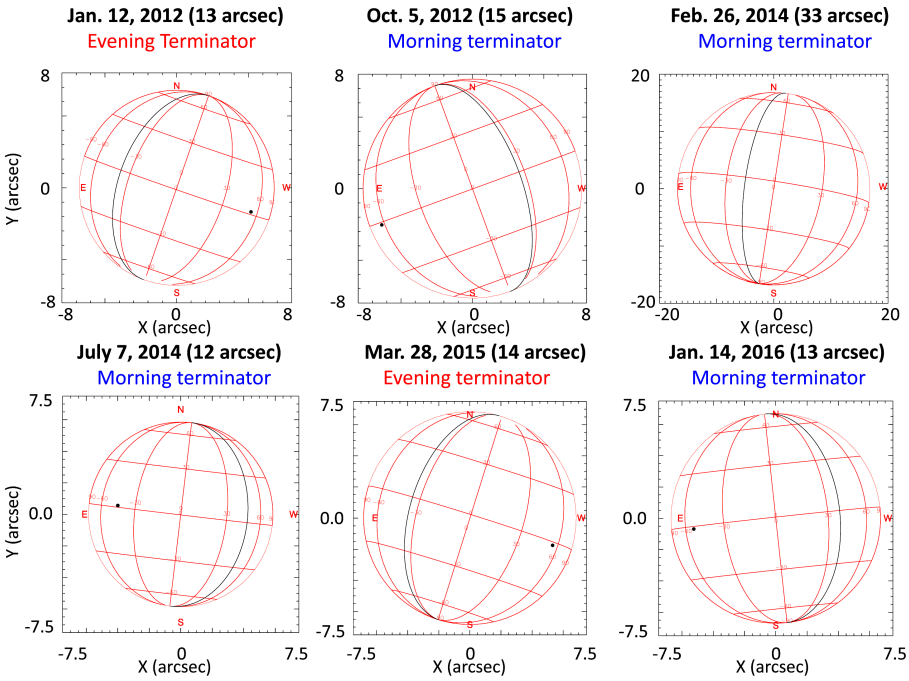

Fig. 1. Geometrical configurations of the disk of Venus during the six TEXES observing runs of 2012–2016. The terminator is indicated by a black line and the subsolar point is shown in black. Two of the runs (January 2012, March 2015) correspond to the evening terminator (night side to the *left* of the terminator), while the four others correspond to the morning terminator (night side to the *right* of the terminator). These two geometrical configurations lead to different thermal structures at high latitudes.

Table 1. Summary of TEXES observations of Venus between January 2012 and January 2016.

Date	Type of obs.	Freq. range (cm^{-1})	Venus diameter (arcsec)	Ill. factor %	Doppler vel. ($km\,s^{-1}$)	Morn/eve term
2012 Jan. 10–12	CO_2, SO_2, HDO	1350–1358	13	80	–10	Evening
	CO_2, SO_2	1362–1370				
	CO_2, SO_2, HDO	1344–1350				
2012 Oct. 4–5	CO_2, SO_2, HDO	1344–1350	15	72.5	+ 12	Morning
	CO_2, SO_2	529–531				
2014 Feb. 26, 28	CO_2, SO_2, HDO	1344–1350	33	35	+ 12	Morning
	CO_2, SO_2 529–531					
	CO_2, SO_2, SO	1155–1158				
	CO_2	787–793				
	CO_2	953–958				
2014 Jul. 6–9	CO_2, SO_2, HDO	1342–1348	12	87	+ 9	Morning
	CO_2, SO_2	529–531				
	CO_2	951–956				
2015 Mar. 27–28	CO_2, SO_2, HDO	1342–1348	14	78	–11	Evening
	CO_2, SO_2, HDO	1350–1355				
	CO_2, SO_2	529–531				
	CO_2	951–956				
2016 Jan. 13–17	CO_2, SO_2, HDO	1342–1348	13	81	+ 10	Morning
	CO_2, SO_2	529–531				
	CO_2	787–793				

corresponding geometry of the Venus disk. The diameter of the planet ranged from 12 arcsec (in July 2014) up to 33 arcsec (in February 2014). The evening terminator was observed twice, in January 2012 and March 2015, while the morning terminator was observed during the four other runs. As discussed in E13, these two configurations lead to very different thermal structures at high latitudes.

In all cases, the slit of the TEXES instrument, aligned along the North–South celestial axis, was shifted from West to East in order to map the planetary disk. The step was half the slit width, i.e. 0.5 arcsec at 7.4 μm, and 0.7 arcsec at 19 μm. Because the slit length (6 arcsec at 7.4 μm, 13 arcsec at 19 μm) was smaller than the Venus diameter at 7.4 μm (and also sometimes at 19 μm), we had to repeat the scan several times in order to map the whole planet. Each scan was recorded in about 6 min so a full map was obtained in 18 to 42 min at 7.4 μm, and 6 to 18 min at 19 μm, depending on the apparent size of the planet. TEXES data cubes are calibrated using the radiometric method commonly used for submillimeter and millimeter astronomy (Rohlfs & Wilson 2004), which is described in detail in Lacy et al. (2002).

Figures 2 and 3 show examples of brightness temperature maps, derived from continuum maps obtained for the six observing runs at 7.4 μm and 19 μm respectively, and Figs. 5 and 6 show maps of the line depth of a weak CO_2 line for the same observations (note that no data at 19 μm were recorded on January 2012). Table 2 list the observing times and durations

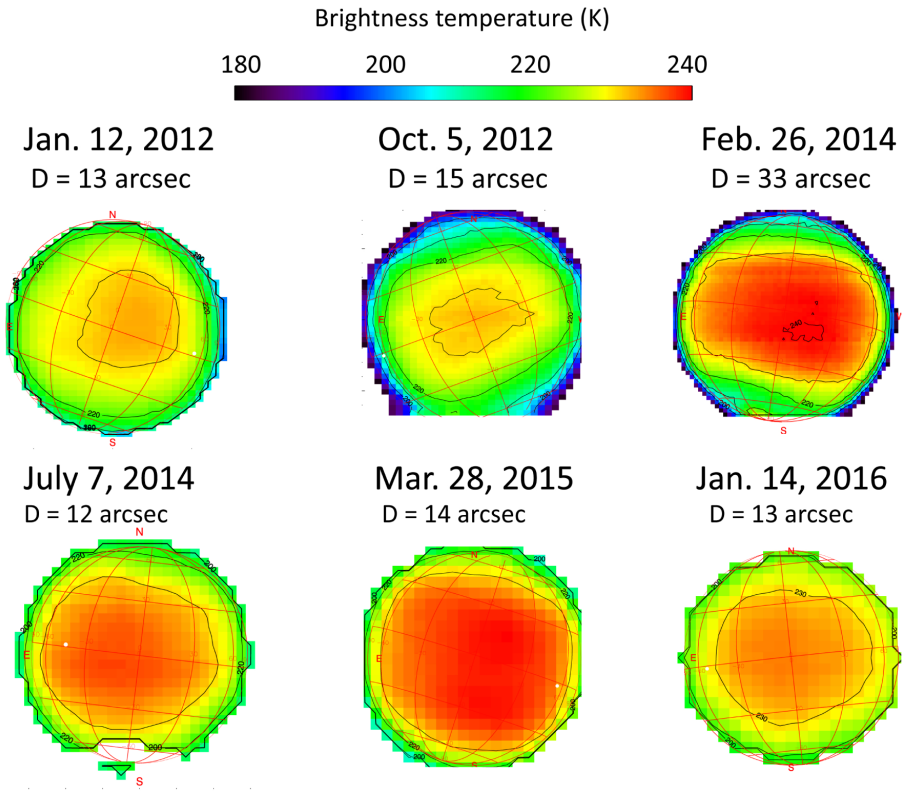

Fig. 2. Examples of brightness temperature maps of Venus, derived from the continuum maps recorded during each of the TEXES observing runs at a frequency of 1345.08 cm^{-1} (7.4 μm). The exact dates and durations of the maps are indicated in Table 2. The scale is the same for all six maps. A brightness temperature of 235 K corresponds to a radiance of 7.44 erg/s/cm^2/sr/cm^{-1} at 1345 cm^{-1}.

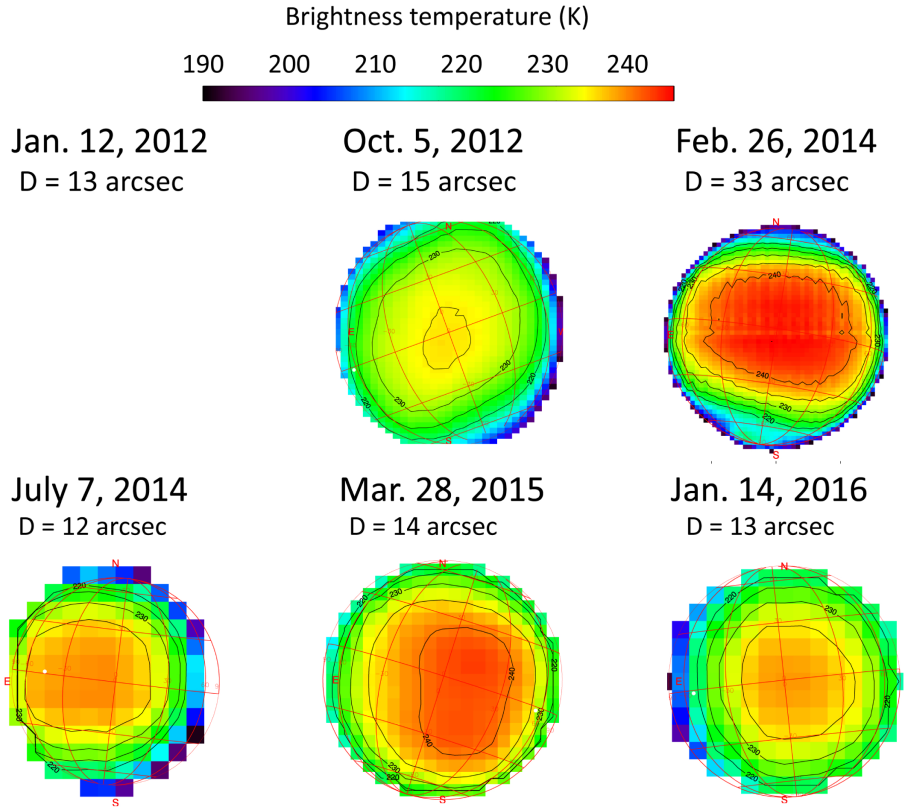

Fig. 3. Examples of brightness temperature maps of Venus, derived from the continuum maps recorded during each of the TEXES observing runs at a frequency of 529.28 cm^{-1} (18.9 μm). The exact dates and durations of the maps are indicated in Table 2. The scale is the same for all six maps. A brightness temperature of 235 K corresponds to a radiance of 71.9 erg/s/cm^2/sr/cm^{-1} at 530 cm^{-1}. No data were acquired at 19 μm in January 2012.

of each map. The brightness temperature indicates the penetration level of the radiation, at 7.4 μm and 19 μm respectively. As expected from the above discussion, the 19 μm temperatures are higher by a few degrees as compared with the ones at 7.4 μm. The brightness temperature maps are globally homogeneous and isotropic, with no apparent variation between the day side and the night side. They show some intensity variations from one run to another, by as much as 20% in radiance at 7.4 μm, and 10% in radiance at 19 μm; part of these differences might be due to the instrumental uncertainty in measuring absolute radiances. When the morning terminator is observed, the continuum maps show a drop at high latitude corresponding

Table 2. Observing times and durations of the observations shown in Figs. 3–20.

Date	Time (UT)	Venus diameter (arcsec)	Molecule	Frequency range (cm^{-1})	Doppler shift (cm^{-1})	Duration (minutes)
Jan. 12, 2012	03:00	13	CO_2, SO_2, HDO	1344.9–1345.4	+ 0.045	18
Oct. 5, 2012	16:55	15	CO_2, SO_2, HDO	1344.9–1345.4	–0.054	18
Oct. 5, 2012	19:40	15	CO_2, SO_2	529–531	–0.020	12
Oct. 5, 2012	18:35	15	CO_2, SO_2, HDO	1344.9–1345.4	–0.054	18
Oct. 5, 2012	20:10	15	CO_2, SO_2	529–531	–0.020	12
Feb. 26, 2014	17:35	33	CO_2, SO_2, HDO	1344.9–1345.4	–0.054	42
Feb. 26, 2014	19:09	33	CO_2, SO_2	529–531	–0.020	18
Jul. 7, 2014	16:49	12	CO_2, SO_2, HDO	1344.9–1345.4	–0.040	12
Jul. 7, 2014	18:09	12	CO_2, SO_2	529–531	–0.016	6
Jul. 7, 2014	18:55	12	CO_2, SO_2, HDO	1344.9–1345.4	–0.040	12
Jul. 8, 2014	16:42	12	CO_2, SO_2, HDO	1344.9–1345.4	–0.040	12
Jul. 8, 2014	17:47	12	CO_2, SO_2, HDO	529–531	–0.016	6
Jul. 8, 2014	18:31	12	CO_2, SO_2, HDO	529–531	–0.016	6
Jul. 8, 2014	19:30	12	CO_2, SO_2, HDO	1344.9–1345.4	–0.040	12
Mar. 28, 2015	23:19	14	CO_2, SO_2, HDO	529–531	+ 0.050	12
Mar. 28, 2015	00:21	14	CO_2, SO_2, HDO	1344.9–1345.4	+ 0.019	18
Jan. 13, 2016	18:05	13	CO_2, SO_2, HDO	1344.9–1345.4	–0.045	18
Jan. 13, 2016	19:09	13	CO_2, SO_2	529 -531	–0.018	12
Jan. 13, 2016	19:51	13	CO_2, SO_2, HDO	1344.9–1345.4	–0.045	18
Jan. 13, 2016	20:30	13	CO_2, SO_2	529–531	–0.018	12
Jan. 14, 2016	18:01	13	CO_2, SO_2, HDO	1344.9–1345.4	–0.045	18
Jan. 14, 2016	18:39	13	CO_2, SO_2	529–531	–0.018	12
Jan. 14, 2016	19:09	13	CO_2, SO_2, HDO	1344.9–1345.4	–0.045	18
Jan. 14, 2016	19:55	13	CO_2, SO_2	529–531	–0.018	12
Jan. 14, 2016	20:33	13	CO_2, SO_2, HDO	1344.9–1345.4	–0.045	18
Jan. 14, 2016	21:11	13	CO_2, SO_2	529–531	–0.018	12
Jan. 15, 2016	18:01	13	CO_2, SO_2, HDO	1344.9–1345.4	–0.045	18
Jan. 15, 2016	18:44	13	CO_2, SO_2	529–531	–0.018	12
Jan. 15, 2016	19:13	13	CO_2, SO_2, HDO	1344.9–1345.4	–0.045	18
Jan. 15, 2016	20:03	13	CO_2, SO_2	529–531	–0.018	12
Jan. 15, 2016	20:37	13	CO_2, SO_2, HDO	1344.9–1345.4	–0.045	18
Jan. 15, 2016	21:18	13	CO_2, SO_2	529–531	–0.018	12
Jan. 16, 2016	19:33	13	CO_2, SO_2, HDO	1344.9–1345.4	–0.045	18
Jan. 16, 2016	20:13	13	CO_2, SO_2	529–531	–0.018	12
Jan. 16, 2016	20:46	13	CO_2, SO_2, HDO	1344.9–1345.4	–0.045	18
Jan. 17, 2016	18:04	13	CO_2, SO_2, HDO	1344.9–1345.4	–0.045	18
Jan. 17, 2016	18:50	13	CO_2, SO_2	529–531	–0.018	12
Jan. 17, 2016	19:44	13	CO_2, SO_2, HDO	1344.9–1345.4	–0.045	18
Jan. 17, 2016	20:21	13	CO_2, SO_2	529–531	–0.018	12
Jan. 17, 2016	20:44	13	CO_2, SO_2, HDO	1344.9–1345.4	–0.045	18

to the polar collar, also associated with a decrease of the temperature gradient over the penetration level. This previously observed effect has been interpreted as the signature of a diurnal cold wave at high latitude (Migliorini et al. 2012; Yamamoto & Takahashi 2012; E13). This effect is absent, as observed in the 2012 TEXES observations and confirmed later, when the evening terminator is observed (January 2012, March 2015). We must point out, however, that this effect is clearly visible in three runs corresponding to the morning terminator (October 2012, February 2014, July 2014), but is significantly weaker on the last one (January 2016). Figures 4 and 5 illustrate that, when the morning terminator is observed, at latitudes above 60°, the temperature gradient upon the penetration level can be null or negative, which implies that the thermal profile becomes isothermal or shows an inversion. In this case, the retrieval of the SO_2 and HDO mixing ratios is no more reliable.

Figures 4 and 5 also show that the thermal gradient above the cloudtop, measured from the line depth of the CO_2 transition, shows some variations over the different cycles. At 7.4 μm, while it is more or less constant from January 2012 to July 2014, it shows a significant decrease of about 20% in March 2015 and January 2016; at 19 μm, the CO_2 line depth is stronger in February and July 2014. These fluctuations apparently reflect temporal variations of the thermal profile.

At 7.4 μm, we have selected the 1344.8–1345.4 cm^{-1} range, which has the advantage of showing two SO_2 multiplets (around 1345.12 and 1345.28 cm^{-1}) bracketing a weak CO_2 transition (at 1345.22 cm^{-1}), all free of terrestrial contamination whatever the Doppler shift is. A HDO transition is present at 1344.9 cm^{-1}, on the wing of a broad terrestrial absorption which shifts in frequency as a function of the Doppler velocity and shows a variable intensity, depending of the water amount in the terrestrial atmosphere. Figure 6 shows a selection of six representative spectra corresponding to the six observing runs. It can be seen that the terrestrial contamination was especially strong in the October 2012 spectrum, as already pointed out in E13. In

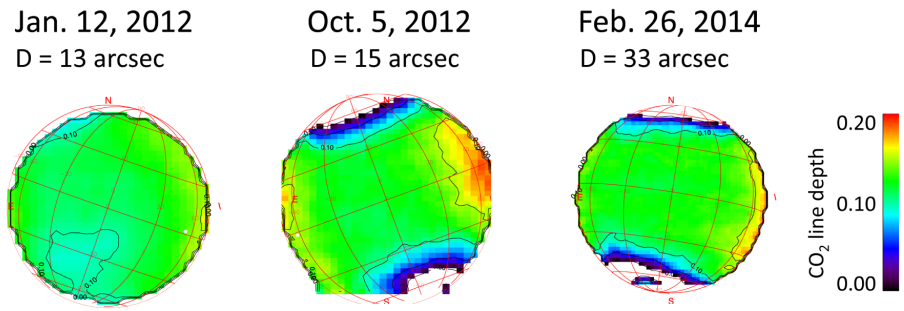

Fig. 4. Examples of maps of the line depth of a weak CO_2 transition at 1345.22 cm^{-1} (7.4 μm) recorded during each of the TEXES observing runs. The exact dates and durations of the maps are indicated in Table 2. The scale is the same for the 6 maps.

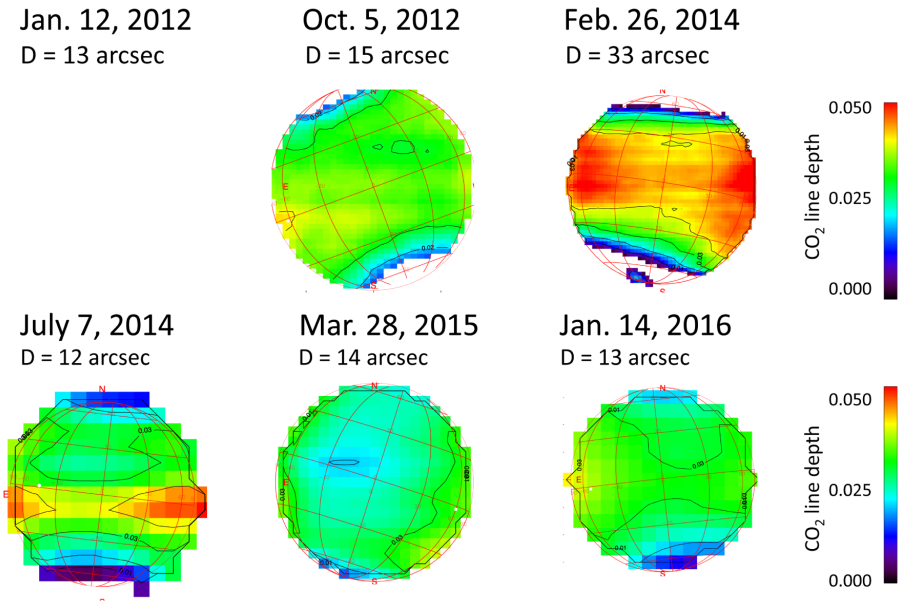

Fig. 5. Examples of maps of the line depth of a weak CO_2 transition at 529.26 cm^{-1} (18.9 μm) recorded during each of the TEXES observing runs. The exact dates and durations of the maps are indicated in Table 2. The scale is the same for the 6 maps. No data were acquired at 19 μm in January 2012.

the 19-μm region, the spectral range covered by the TEXES instrument is much smaller than at 7.4 μm, and the different Fabry-Perot orders do not overlap. Figure 7 shows two spectral intervals, at 529.1–529.4 cm^{-1} and at 529.65–530.0 cm^{-1}. Both intervals contain weak multiplets of SO_2 and weak CO_2 transitions.

The SO_2 absorption features, compared with the CO_2 lines, show significant variations from a run to another, both at 7.4 μm and at 19 μm. The SO_2 lines were strongest in the January 2016 data, while they were almost undetectable in the February 2014 data.

2.2. Atmospheric modeling

Our synthetic spectra of Venus were calculated using a line-by-line radiative transfer code without scattering, also used in our previous analyses (E12, E13). We neglected the effect of scattering which, at mid-infrared wavelengths, is expected to be very small. Indeed, based on the cloud model of Crisp (1986), using mode 1 and 2 spherical particles with a H_2SO_4 concentration of 75%, we derive for the mean single scattering albedo a value of 0.075 for wavelengths of both 7.4 and 19 μm. The line intensities of the CO_2, SO_2 and HDO transitions at 7.4 μm, as well as the CO_2 lines at 19 μm, were taken from the GEISA database (Jacquinet-Husson et al. 2008). For SO_2 at 19 μm, we used the line intensities of Rothman et al. (2005). Indeed, we noticed for the relative intensities of SO_2, a better agreement with the TEXES data when using this database rather than the GEISA one. The self-broadening coefficients of CO_2 were taken from GEISA. In the case of SO_2 and HDO, following Nakazawa & Tanaka (1982), we multiplied the GEISA broadening coefficient by N_2 by a factor 1.4. For the temperature dependence of the broadening coefficients, we used $n = -0.75$ for CO_2 and SO_2 (Bézard et al. 1990) and −0.35 for HDO (Varanasi 1971). Table 3 lists the spectrospic parameters of the lines used for the SO_2 and HDO mapping.

As a nominal thermal profile (corresponding to low and mid latitudes), we first considered the thermal profile inferred from our 2012 observations (E13). This profile was retrieved from the

Table 3. Spectroscopic parameters of the transitions used for the HDO and CO_2 mapping and for the spectral fits.

Molecule	Wavenumber (cm^{-1})	QN(band)	QN(line)	S ($cm\ mol^{-1}$)	E (cm^{-1})	Broad. coef. ($cm^{-1}\ atm^{-1}$)	n
HDO	1344.899	010 000	303 404	1.62×10^{-23}	150.2	0.133	–0.35
SO_2	1345.096	011 010	27 25 2 27 25 3	2.11×10^{-21}	712.4	0.140	–0.75
SO_2	1345.108	001 000	26 1 26 27 1 27	4.10×10^{-20}	229.5	0.143	–0.75
SO_2	1345.126	001 00	23 7 16 24 7 17	2.62×10^{-20}	275.2	0.143	–0.75
SO_2	1345.137	001 000	21 11 10 22 11 11	1.25×10^{-20}	367.1	0.143	–0.75
SO_2	1345.141	011 010	16 9 8 17 9 9	1.38×10^{-21}	756.5	0.140	–0.75
SO_2	1345.282	001 000	24 3 22 25 3 23	3.80×10^{-20}	223.05	0.143	–0.75
SO_2	1345.285	001 000	17 16 1 18 16 2	1.21×10^{-21}	541.3	0.143	–0.75
CO_2	1345.219	100 01 000 01	R3E	4.20×10^{-27}	4.4	0.119	–0.75
SO_2	529.310	010 000	20 4 16 20 3 17	3.53×10^{-21}	160.0	0.143	–0.75
SO_2	529.315	010 000	28 2 26 28 1 27	2.15×10^{-21}	261.0	0.143	–0.75
SO_2	529.324	010 000	23 3 21 23 2 22	2.82×10^{-21}	180.6	0.143	–0.75
SO_2	529.327	010 000	19 1 19 18 0 18	6.69×10^{-21}	105.3	0.143	–0.75
SO_2	529.314	010 000	431 322	1.61×10^{-21}	10.7	0.143	–075
CO_2	529.261	111 02 100 01	P9E	1.13×10^{-26}	1399.0	0.110	–0.75

Notes. SO_2 transitions weaker than $1.0\ 10^{-21}$ $cm\ mol^{-1}$ have been omitted from the Table, but they have been included in the calculation of the synthetic spectra.

study of both weak and strong CO_2 transitions in the TEXES spectra taken in October 2012. As discussed in E13, it showed some departure from the VIRA low-latitude profile, with a lower temperature at the cloudtop (z = 60 km in E13), and a lower gradient above this level. It was, however, closer to the thermal profile derived from the VIRTIS-M data at 4.7 μm (Irwin et al. 2008). In the E13 model, the temperature was 241 K at the 19-μm penetration level (z = 57 km, Ps = 250 mbar), and 231 K at the 7.4-μm penetration level (z = 61 km, Ps = 100 mbar). In the mesosphere, temperatures were 215 and 192 K at altitudes of 70 km and 80 km respectively. In the present study, we have used a thermal profile intermediate between E13 and VIRA as a first guess, and we have adjusted the pressure scales and the mean temperatures of the penetration levels, at 7.4 and 19 μm respectively, in order to fit the disk-integrated spectra of February 26, 2014 and January 14, 2016 (see Sect. 3.1).

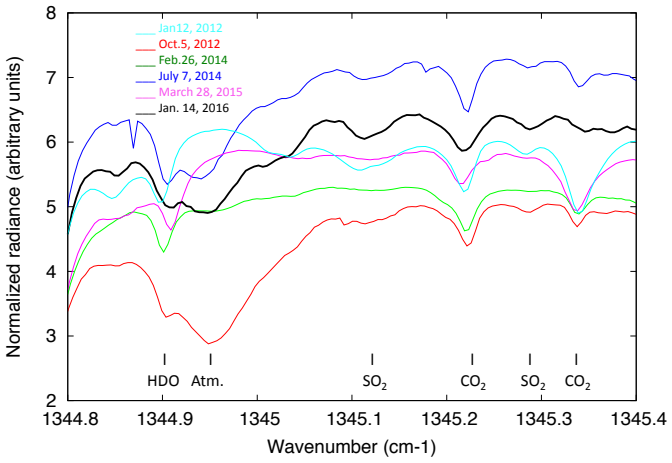

Fig. 6. Examples of disk-integrated spectra recorded during each of the TEXES observing runs between 1344.8 and 1345.4 cm^{-1} (7.4 μm). The exact dates and durations of the corresponding observations are indicated in Table 2. It can be seen that the SO_2 absorption bands are strongest in January 2016, and weakest in February 2014.

3. Results

3.1. SO_2 variability

Figures 8 and 9 illustrate the variability of the SO_2 volume mixing ratio above and within the clouds between January 2012 and January 2016. Examples have been taken for each of the six runs, corresponding to the same maps as for the continuum and the CO_2 line depth (Figs. 2–5). The SO_2 content is inhomogeneous over the disk, both at the cloudtop (7 μm map) and a few kilometers below within the clouds (19 μm map), as already stated in our previous analyses (E12, E13). Comparison with Fig. 1 shows that there is no evidence for a difference between the dayside and the nightside. The 19-μm maps are of lower quality than the 7.4-μm because of two reasons: (1) the spatial resolution is lower; and (2) the continuum shows a curvature (Fig. 7) which may slightly change over the disk, and introduces some uncertainty in the retrieval of the SO_2 volume mixing ratio within the clouds. This uncertainty in the continuum may actually induce an artifact in this measurement, as was probably the case in our measurements of October 4, 2012 (E13). In E13, we announced a short-term variation of the SO_2 content within the clouds between two maps separated by 30 min. After examining data from other runs since 2012, we now attribute this variation to an instrumental artifact due to a change in the continuum slope curvature at 529.7 cm^{-1}. Because of this potential problem, we consider that the 19-μm data should be considered with special caution.

Both Figs. 8 and 9 illustrate that the SO_2 content exhibits very strong long-term temporal variations at the cloudtop and within the clouds over a timescale of four years, confirming the tendency shown in the disk-integrated spectra (Figs. 6 and 7). The strongest difference is observed between the February 2014

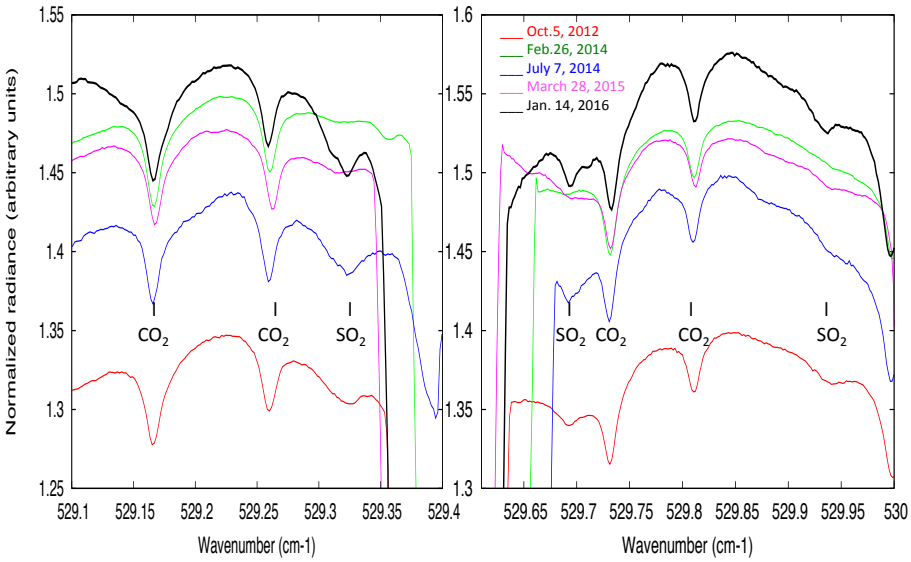

Fig. 7. Examples of disk-integrated spectra recorded during each of the TEXES observing runs in the 18.9-μm range. *Left*: 529.1–529.4 cm^{-1}; *right*: 529.65–530 cm^{-1}. The exact dates and durations of the corresponding observations are indicated in Table 2. It can be seen that the SO_2 absorption bands are strongest in January 2016, and weakest in February 2014.

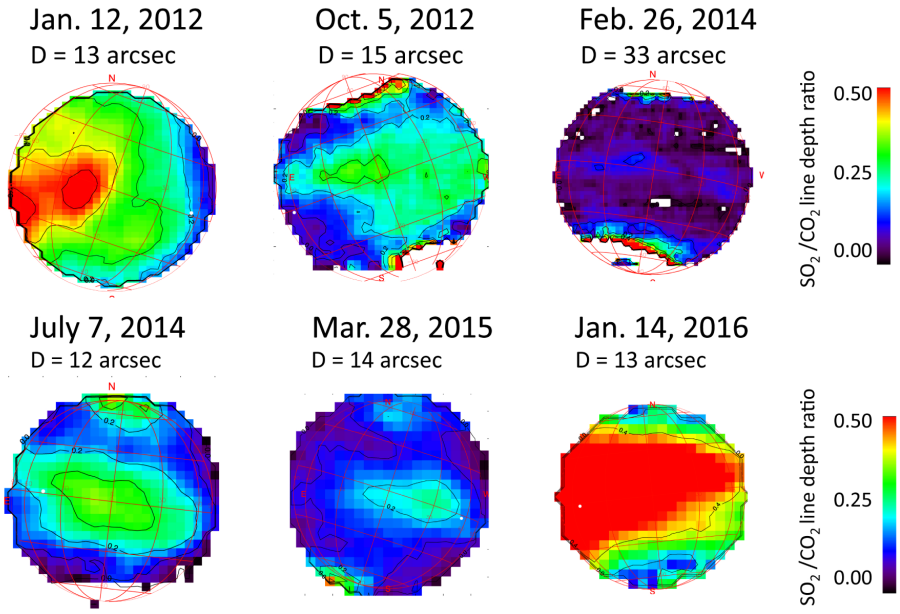

Fig. 8. Example maps of the line depth ratio of a weak SO_2 multiplet around 1345.11 cm^{-1} (7.4 μm) divided by a weak CO_2 transition at 1345.22 cm^{-1}, recorded during each of the TEXES observing runs. The scale is the same for the six maps. The exact dates and durations of the maps are indicated in Table 2.

maps, which correspond to a minimum SO_2 content, and the January 2016 maps where the SO_2 content is maximum.

In order to better follow the short-term variations of SO_2, we have recorded a sequence of maps between January 13 and January 17, with two or three maps per day at both 7.4 and 19 μm, separated by 1 to 2 h each day. Results are shown in Figs. 10 and 11 respectively. We recall that the four-days rotation of the clouds at the cloudtop makes the SO_2 features (if associated with clouds) shift by 90 deg over a 24-h period. It is thus not surprising that the SO_2 morphology drastically changes from a day to the next one. A rotation of two hours translates into a shift of 7.5 deg at the equator. Such shift is observed between the three 7.4-μm maps of January 14, 2016 and also (although less clearly) on the three maps of January 17. The effect is slightly visible on the January 14 maps (and possibly the January 15 maps) at 19 μm.

For a better analysis of the correlation between the motion of the SO_2 features at the cloudtop and the four-day retrograde rotation, we have selected in our dataset a few examples where such correlation is clearly visible. These maps, shown in Fig. 12, correspond to data recorded on July 7, 2014, July 8, 2014 and January 14, 2016; they are separated each time by about two hours. The shift by 7.5 deg is actually visible in these three cases. On the other hand, there are also examples (as shown in Fig. 10 on January 13, 2016 and in Fig. 12 on July 8, 2014) where real changes seem to take place at the cloudtop within a timescale of two hours. We thus conclude that the lifetime of the SO_2 features at the cloudtop is of the order of a few hours.

In order to obtain an absolute calibration of the SO_2 volume mixing ratio as a function of the SO_2/CO_2 line depth ratio, we modeled two disk-integrated spectra corresponding to a minimum SO_2 value (Feb. 26, 2014) and a maximum SO_2 value (Jan. 14, 2016), both at 7.4 μm and at 19 μm. Figures 13 and 14 show the two SO_2 spectra recorded at 1345 cm^{-1} (7.4 μm). To determine the thermal profile, as a first guess we took a profile intermediate between E13 and VIRA (see Sect. 2) and adjusted the pressure scales and mean temperatures of the penetration levels to fit the weak CO_2 lines of the disk-integrated spectra. Our inferred profile, used for both the February 2014 and the January 2016 datasets, has the following parameters: T = 240 K for P = 210 mbar (z = 60 km), T = 230 K for P = 100 mbar (z = 64 km), T = 220 K for P = 47 mbar (z = 68 km) and

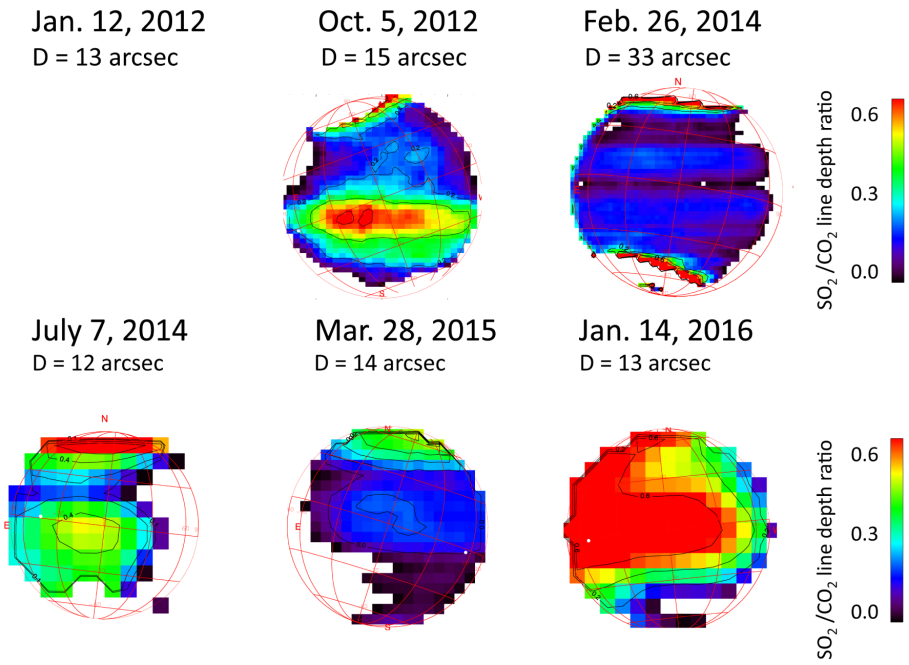

Fig. 9. Example maps of the line depth ratio of a weak SO_2 multiplet at 529.33 cm^{-1} (18.9 μm) divided by a weak CO_2 transition at 529.26 cm^{-1}, recorded during each of the TEXES observing runs. The scale is the same for the six maps. The exact dates and durations of the maps are indicated in Table 2.

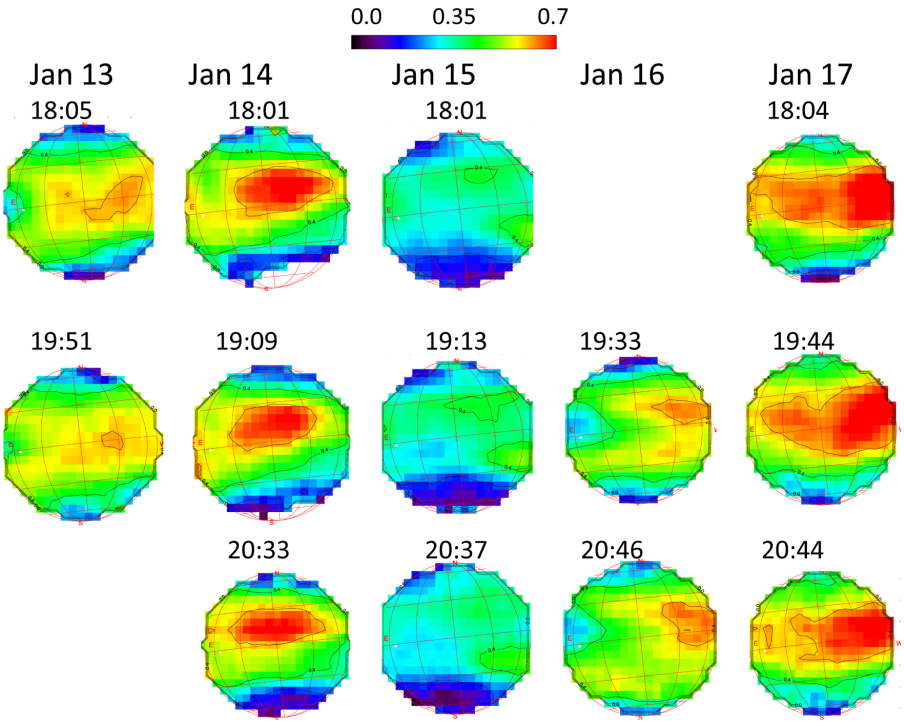

Fig. 10. Maps of the line depth ratio of a weak SO_2 multiplet around 1345.11 cm^{-1} (7.4 μm) divided by a weak CO_2 tr ansition at 1345.22 cm^{-1}, recorded with TEXES between January 13 and January 17, 2016. The scale is the same for all maps. The exact dates and durations of the maps are indicated in Table 2.

T = 200 K at P = 7 mbar (z = 77 km). We note that this profile is not a unique solution; it is simply used as a tool to model the weak CO_2 lines of the disk-integrated spectra. The same thermal profile was used for the 7.4-μm and the 19-μm data. As in our previous analyses, a cloud of infinite opacity was introduced at the level T = 230 K (P = 100 mbar, z = 64 km) for the 7.4-μm data, and at the level T = 240 K (P = 210 mbar, z = 60 km). Using the same thermal profile (adequate for low latitudes) for all latitudes induces an error at high latitudes, especially in the case of the four datasets corresponding to morning terminator observations. As mentioned above, the mixing ratios retrieved at high latitude in this case should be discarded anyway because of the temperature inversion occurring above 60° latitude.

We note that we have no information on the absolute altitude scale. In the present study, we have inferred the altitude scale from the pressure scale, using the VIRA low-latitude profile as a reference (with the VIRA pressure level of 100 mbar corresponding to an altitude of 64 km). Our altitude scale is thus slightly shifted (by +4 km) with respect to the one indicated in E13. At low latitudes and in the lower mesosphere, the VIRA profile is very close to the more recent VeRa profile obtained by the Radio science experiment aboard Venus Express; between 60 and 75 km, temperature differences between VIRA and VeRa profiles are less than 5 K (Tellmann et al. 2009).

We also needed an assumption about the vertical distribution of SO_2. Our previous analysis (E13) indicated a cut-off of the

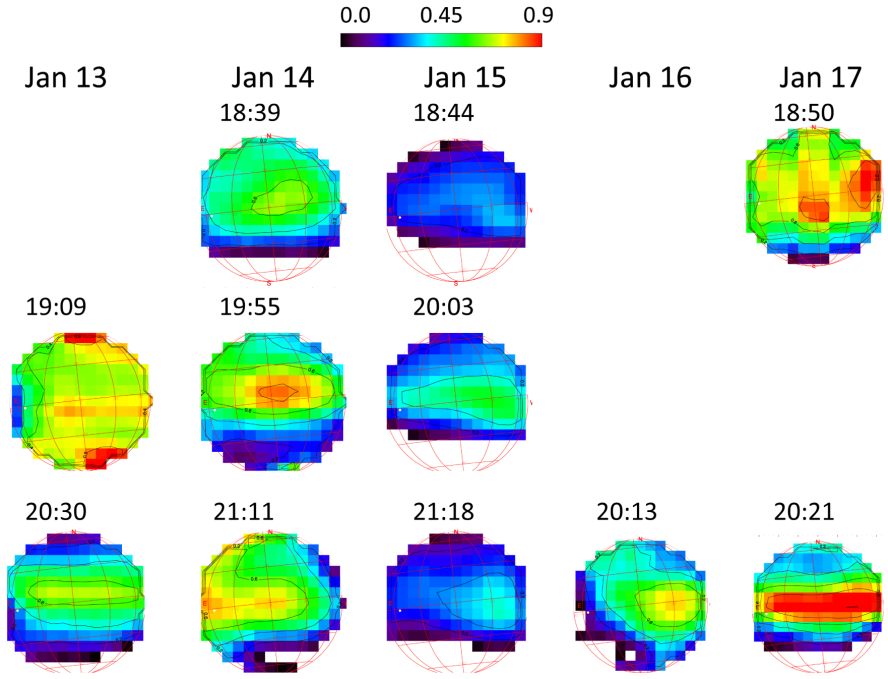

Fig. 11. Maps of the line depth ratio of a weak SO_2 multiplet around 529.33 cm^{-1} (18.9 μm) divided by a weak CO_2 tr ansition at 529.26 cm^{-1}, recorded with TEXES between January 13 and January 17, 2016. The scale is the same for all maps. The exact dates and durations of the maps are indicated in Table 2.

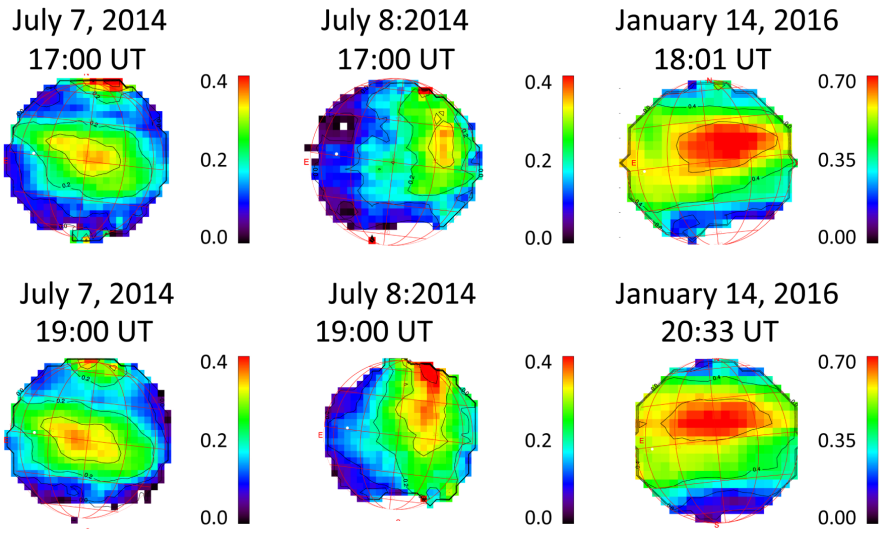

Fig. 12. Examples of maps of the line depth ratio of a weak SO_2 multiplet around 1345.11 cm^{-1} (7.4 μm) divided by a weak CO_2 tr ansition at 1345.22 cm^{-1}, separated by about 2 h, recorded with TEXES on July 7, 2014, July 8, 2014, and January 14, 2016. The exact dates and durations of the maps are indicated in Table 2.

SO_2 distribution at the z = 67 km level (in the E13 profile), corresponding to a temperature of 220 K. In order to reduce all data in an homogeneous way, we have assumed the same cut-off, at z = 68 km (T = 200 K, P = 47 mbar, new profile) for all observations between 2012 and 2016. The validity of this assumption is discussed in Sect. 4.

As shown in Figs. 13 and 14, the data of Feb. 26, 2014 are best fitted with a SO_2 volume mixing ratio of 30 ppbvv, while the data from Jan. 14, 2016 are best fitted with a SO_2 value of 300 ppbv, that is, ten times stronger. Figures 15 and 16 show the fits obtained, at 19 μm, for the SO_2 spectra of February 26, 2014 and January 14, 2016 respectively. They confirm the results obtained at 7.4 μm. At both 7.4 and 19 μm, best fits are obtained with a SO_2 volume mixing ratio of 30 ppbv on Feb. 26, 2014 and 300 ppbv on January 14, 2016. The factor of ten difference between the two datasets confirms the results shown in Figs. 8 and 9. The uncertainty on the SO_2 volume mixing ratios is discussed in Sect. 4. Figures 13–16 also show a synthetic spectrum of SO_2 corresponding to a constant vertical mixing ratio. In the case of the 7-μm data, it is not possible to discriminate between the two vertical distributions, with and without the cutoff, as we did using the data of October 2012 (E13). This is because the spectral resolution (0.024 and 0.028 cm^{-1} for the February 2014 and January 2016 data respectively) is not as good as for the October 2012 observations (0.016 cm^{-1}). In contrast, at 19 μm, the spectral resolution of 0.010 cm^{-1}, obtained for all datasets, allows us to show that a better fit is obtained when a cutoff is introduced. We note that the altitude of this cutoff is significantly lower than the region where SO_2 has been found to increase again (above z = 85 km), as shown by millimeter and submillimeter observations (Sandor et al. 2010, 2012; Encrenaz et al. 2015b). The TEXES observations are not sensitive to the upper mesosphere where the pressure is lower than 1 mbar.

3.2. HDO variability

Figure 17 shows series of six HDO maps representative of our six observing runs between January 2012 and January 2016. These maps are extracted from the same data as shown in Figs. 2, 4 and 8 for the continuum, the CO_2 line depth and the

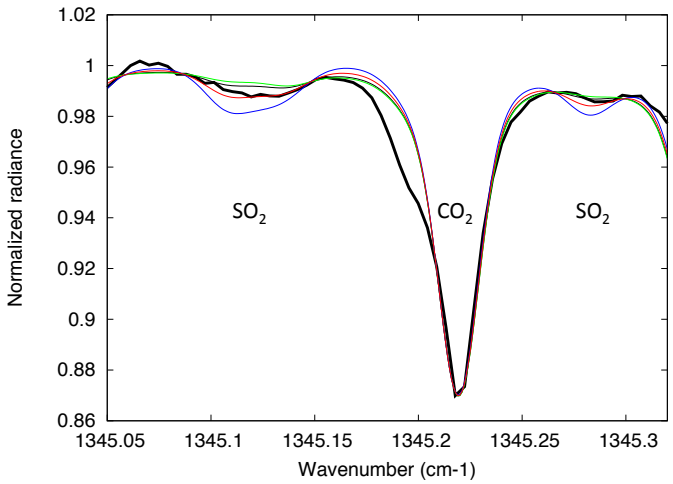

Fig. 13. Disk-integrated spectrum recorded by TEXES on February 26, 2014, between 1345.05 and 1345.32 cm^{-1} (7.4 μm), showing weak transitions of CO_2 and SO_2. The date and duration of the corresponding observation are indicated in Table 2. The February 2014 run corresponds to the weakest SO_2 content measured at the cloupdtop between 2012 and 2016. Thick black line: TEXES data; thin lines: models. Green: SO_2 = 20 ppbv with cutoff; red (best fit): SO_2 = 30 ppbv with cutoff; blue: SO_2= 40 ppbv with cutoff; black: SO_2 = 15 ppbv, constant with altitude. The spectral resolution is 0.024 cm^{-1}.

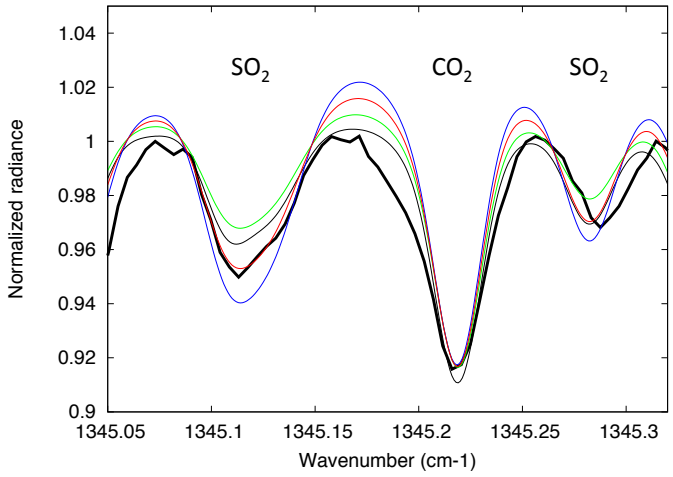

Fig. 14. Disk-integrated spectrum recorded by TEXES on January 14, 2016 (20:33 UT), between 1345.05 and 1345.32 cm^{-1} (7.4 μm), showing weak transitions of CO_2 and SO_2. The date and duration of the corresponding observation are indicated in Table 2. The January 2016 run corresponds to the strongest SO_2 content measured at the cloudtop between 2012 and 2016. Thick black line: TEXES data; thin lines: models. Green: SO_2 = 200 ppbv with cutoff; red (best fit): SO_2 = 300 ppbv with cutoff; blue: SO_2 = 400 ppbv with cutoff; black: SO_2 = 100 ppbv, constant with altitude. The spectral resolution is 0.028 cm^{-1}.

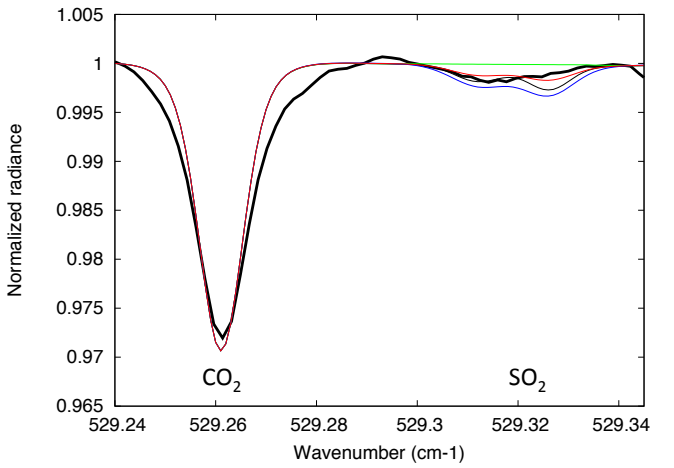

Fig. 15. Disk-integrated spectrum recorded by TEXES on February 26, 2014, between 529.24 and 529.345 cm^{-1} (19 μm), showing weak transitions of CO_2 and SO_2. The date and duration of the corresponding observation are indicated in Table 2. The February 2014 run corresponds to the weakest SO_2 content measured at the cloupdtop between 2012 and 2016. Thick black line: TEXES data; thin lines: models. Green: SO_2 = 0 ppbv; red (best fit): SO_2 = 30 ppbv with cutoff; blue: SO_2 = 60 ppbv with cutoff; black: SO_2 = 8 ppbv, constant with altitude. The quality of the fit is limited by the uncertainty on the continuum curvature and the weakness of the SO_2 band. The spectral resolution is 0.010 cm^{-1}.

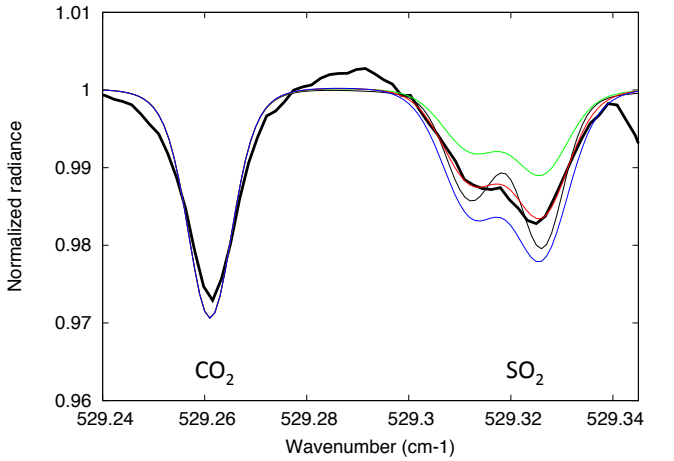

Fig. 16. Disk-integrated spectrum recorded by TEXES on January 14, 2016, between 529.24 and 529.345 cm^{-1} (19 μm), showing weak transitions of CO_2 and CO_2. The date and duration of the corresponding observation are indicated in Table 2. The January 2016 run corresponds to the strongest SO_2 content measured at the cloupdtop between 2012 and 2016. Thick black line: TEXES data; thin lines: models. Green: SO_2 = 200 ppbv with cutoff; red (best fit): SO_2 = 300 ppbv with cutoff; blue: SO_2 = 400 ppbv with cutoff; black: SO_2 = 65 ppbv, constant with altitude. The spectral resolution is 0.010 cm^{-1}.

SO_2 volume mixing ratio, respectively (see Table 2). As we noticed in our previous analyses (E12, E13), the HDO maps are more or less homogeneous over the disk, with a mean variation of a factor 30−50%. As in the case of the SO_2 maps, we consider that the high latitude values have to be regarded with caution, because of the possible uncertainty associated with the temperature profile. We also observe moderate long-term variations. The lowest HDO abundance is measured in January 2016, corresponding to a H_2O volume mixing ratio (vmr) of 1.2 ppmv, while the highest value is found in a single measurement of March 2015 (corresponding to a H_2O vmr of 2.2 ppmv). These variations are only by a factor of two at most, to be compared with the factor of ten observed in the case of the SO_2 abundance at the cloudtop. The possible origin of these fluctuations is discussed in Sect. 4.

The relative uniformity of the HDO distribution over the disk is also illustrated in Fig. 18, which shows the sequence recorded between January 13 and January 17. The data are the same as for the SO_2 maps shown in Fig. 11. Figure 18 confirms the relative uniformity of the HDO content over the planetary disk and over a timescale of a few days.

In some cases (in particular in October 2012, July 2014 and January 2016, as shown in Fig. 6), the Doppler shift is such that

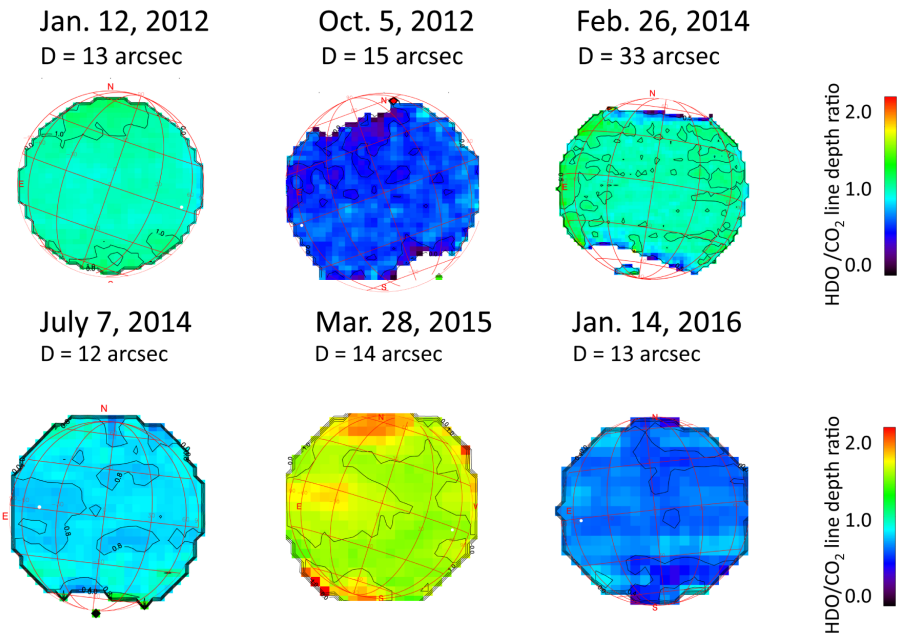

Fig. 17. Examples of maps of the line depth ratio of the HDO transition at 1344.90 cm^{-1} (18.9 μm) divided by a weak CO_2 transition at 1345.22 cm^{-1}, recorded during each of the TEXES observing runs. The data are the same as for Fig. 8. The scale is the same for the six maps. The dates and durations of the maps are indicated in Table 2.

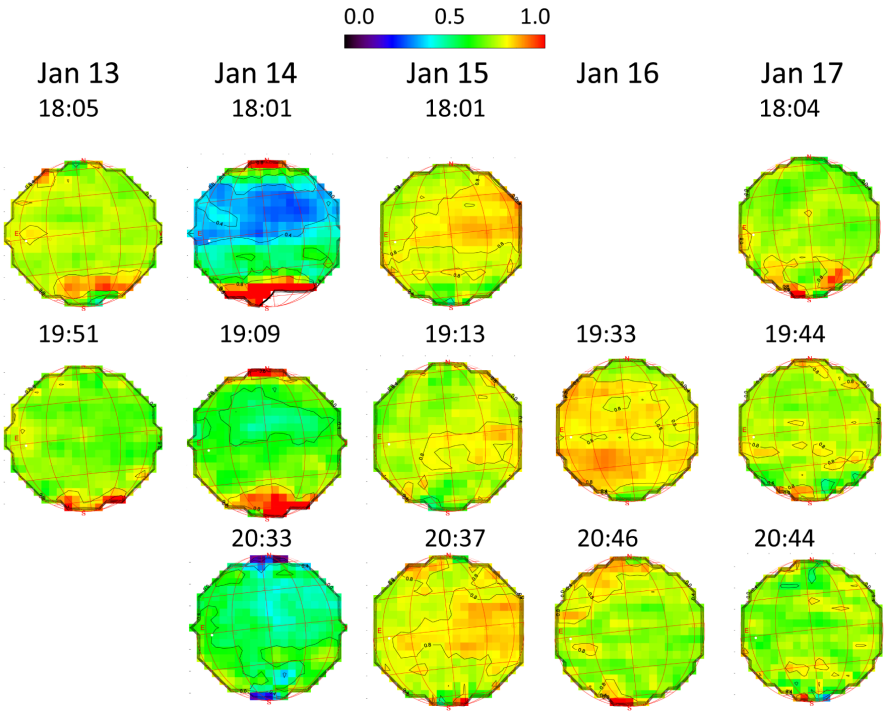

Fig. 18. Maps of the line depth ratio of the HDO transition at 1344.90 cm^{-1} (7.4 μm) divided by a weak CO_2 transition at 1345.22 cm^{-1}, recorded with TEXES between January 13 and January 17, 2016. The data are the same as for Fig. 10. The scale is the same for all maps. The dates and durations of the maps are indicated in Table 2.

the HDO line lies in the wing of a strong terrestrial absorption, making the HDO retrieval more uncertain. In particular, during the January 2016 sequence, short-term fluctuations of the terrestrial water content may have induced an additional uncertainty in the retrievals of the HDO maps. As a consequence, the 20% fluctuations observed on a timescale of two hours on January 16, 2016 (Fig. 18) should be considered with caution.

Figures 19 and 20 show spectral fits of the HDO line extracted from the data corresponding to the minimum and maximum values of the SO_2 volume mixing ratio at the cloudtop (Figs. 13 and 14). To convert the HDO abundances into water abundances, we use a D/H ratio of 200 times the terrestrial VSMOW value (Fedorova et al. 2008). The corresponding H_2O mixing ratios are 1.5 ppmv for February 2014 and 1.0 ppmv for January 2016. Uncertainties are discussed in Sect. 4. We note that, as in the case of the 2012 data (E12, E13), we have assumed a constant vertical distribution for the water mixing ratio in the 60–75 km range, in agreement with previous studies (Gurwell et al. 2007; Fedorova et al. 2008).

4. Discussion

4.1. Uncertainty analysis

In this section, we analyse the uncertainty associated with the mixing ratios shown in the maps and inferred from the fits of the disk-integrated spectra.

There are several possible sources of uncertainty in our results: (1) the instrumental noise of the TEXES data; (2) the

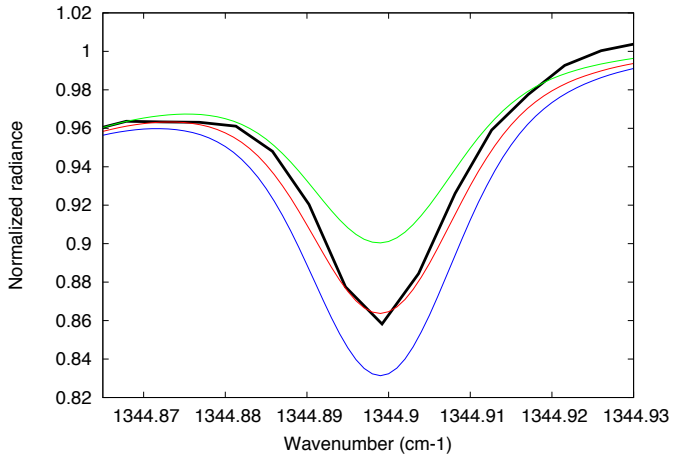

Fig. 19. Disk-integrated spectrum of the HDO transition at 1344.90 cm^{-1} recorded by TEXES on February 26, 2014, (7.4 μm). The dates and durations of the corresponding observation are indicated in Table 2. The February 2014 run corresponds to the weakest SO_2 content measured at the cloupdtop between 2012 and 2016. Thick black line: the TEXES data; thin lines: models. Green: H_2O = 1.0 ppmv; red (best fit): H_2O = 1.5 ppmv; blue: H_2O = 2 ppmv. For the conversion between the HDO and H2O abundances on Venus, we assume a D/H ratio of 200 times the VSMOW (Fedorova et al. 2008).

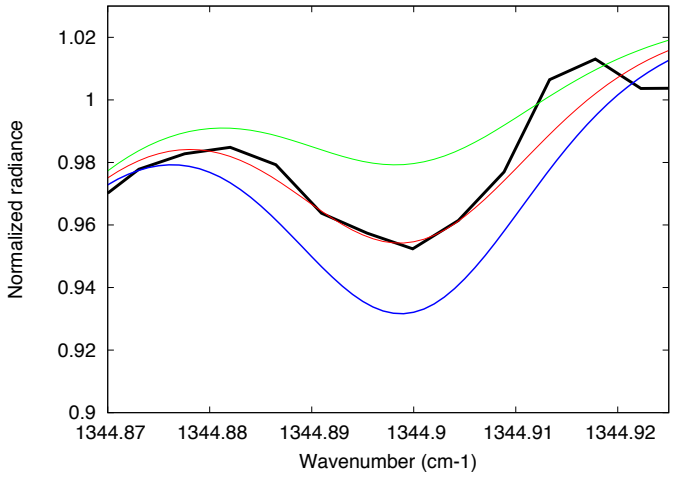

Fig. 20. Disk-integrated spectrum of the HDO transition at 1344.90 cm^{-1} recorded by TEXES on January 14, 2016 (20:33 UT). The date and duration of the corresponding observation are indicated in Table 2. The January 2016 run corresponds to the strongest SO_2 content measured at the cloudtop between 2012 and 2016. Thick black line: the TEXES data; thin lines: models. Green: H_2O = 0.5 ppmv; red (best fit): H_2O = 1.0 ppmv; blue: H_2O = 1.5 ppmv. For the conversion between the HDO and H2O abundances on Venus, we assume a D/H ratio of 200 times the VSMOW (Fedorova et al. 2008).

uncertainty in the continuum of the TEXES spectra; (3) the absolute calibration of the data; and (4) the uncertainty linked with the atmospheric parameters used for calculating the synthetic spectra. The third source (absolute calibration) can be discarded because in the present study, we only consider the line depth ratios of the transitions (in contrast, this effect should be taken into account when we study the thermal structure inferred from the TEXES data). In the case of the fourth source (atmospheric modeling), we can estimate the uncertainty associated with the fact that we infer the mixing ratios of the minor species versus CO_2 from the ratio of their line depth ratios. Previous analyses (Encrenaz et al. 2008, 2012, 2015a) have shown that, in the case of line depths of 10% or less, the departure from linearity may induce an uncertainty of about 10% in the derived mixing ratios.

We now describe our estimation of the instrumental noise of the TEXES data. The (σ) signal-to-noise ratio (S/N) in the continuum of a TEXES disk-integrated spectrum at 1345 cm^{-1} is typically over 1000 per spectral pixel (Figs. 13 and 14). The line depth is typically 0.12 for CO_2 (Figs. 4 and 6), 0.10 for HDO (Fig. 6) and 0.06 for SO_2 (Fig. 6). The line depth is integrated over 8 pixels for the SO_2 multiplet around 1345.12 cm^{-1}, and over 3 pixels for the 1345.28 cm^{-1} SO_2 doublet, the CO_2 and the HDO lines. In the integrated spectrum, the (σ) S/N is thus about 164 for the SO_2 line depth (after summing the two multiplets), 170 for HDO and 200 for CO_2. As a result, the (σ) S/N is about 120 for the SO_2/HDO line depth ratio and 130 for the HDO/CO_2 line depth ratio. For a typical Venus diameter of 14 arcsec, the SO_2 and HDO maps cover an area of about 600 pixels of 0.5 × 0.5 arcsec each. The maps are convolved to a spatial resolution of 1 arcsec. The S/N of the line depth ratio in a spatial element is thus 10 for both SO_2 and HDO. In terms of relative abundances, we can conclude that the SO_2 and HDO mixing ratios within a map are reliable within an uncertainty of 10%.

Another more important limitation is associated with the definition of the TEXES continuum. It can be seen from Figs. 13, 14 and 19–20 that the shapes of the SO_2 and HDO lines are not exactly fitted with the models. We attribute these departures to the uncertainty associated with the continuum level and, in the case of HDO, the uncertainty associated with the correction of the terrestrial absorption. Considering the departure between the data and the synthetic models, and using a D/H ratio of 200 × VSMOV, we derive the following:

February 26, 2014 (Minimum SO_2): SO_2 = 30 +/−5 ppbv, H_2O = 1.5 +/–0.5 ppmv;

January 14, 2014 (Maximum SO_2): SO_2 = 300 +/–50 ppbv, H_2O = 1.0 +/–0.5 ppmv.

In the case of the 19-μm data, the error associated with the instrumental noise becomes negligible because, as shown in Figs. 2 and 3, the flux is ten times stronger than at 7.4 μm. In contrast, the error associated with the definition of the continuum is much stronger, because the SO_2 doublet at 529.32 cm^{-1} lies on a continuum with a strong curvature which may vary over the disk. As a result, the quality of the SO_2 fits is degraded as compared with the 7.4-μm data. Taking this effect into account, we infer:

February 26, 2014 (Minimum SO_2): SO_2 = 30 +/–10 ppbv.

January 14, 2014 (Maximum SO_2): SO_2 = 300 +/–100 ppbv.

Our conclusion is thus that the SO_2 measurements at 19 μm confirm the ones at 7.4 μm, which implies that there is no significant gradient in the SO_2 vertical distribution in the few kilometers above the cloudtop.

4.2. Vertical distribution of SO_2

As mentioned above (Sect. 3.2), the SO_2 volume mixing ratios derived at the cloudtop have been inferred assuming a cutoff in the SO_2 distribution at an altitude of 68 km (corresponding, in our model, to a temperature of 220 K).

Because of our limited spectral resolution which does not allow us to isolate and resolve the individual SO_2 of the multiplets, the quantity that we are measuring is actually not the SO_2 volume mixing ratio at the cloudtop, but the column density above this level. However, it is convenient to convert this quantity into a mixing ratio at the cloudtop, for comparison with other datasets and for the study of temporal variations. We know from

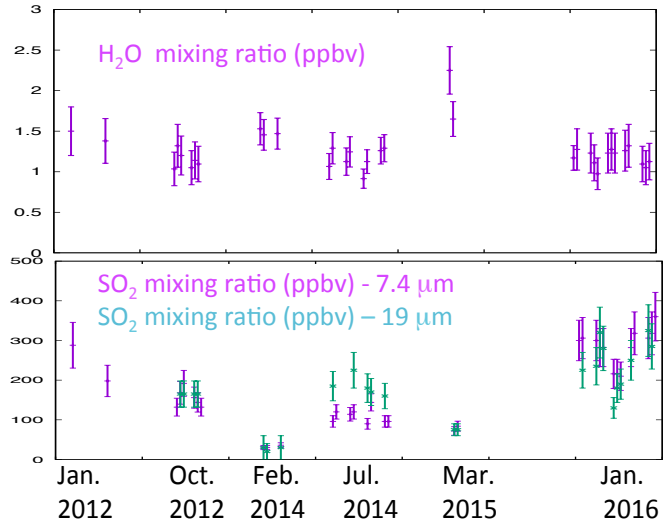

Fig. 21. Long-term variations of the H_2O volume mixing ratio (*top*, measured at 7.4 μm) and the SO_2 volume mixing ratio (*bottom*, measured at 7.4 and 19 μm) between January 2012 and January 2016. The January 2012 and March dataset correspond to evening terminator observations; the 4 other datasets correspond to morning terminator observations. All data were obtained using the lines listed in Table 3, with the exception of the first HDO measurement (January 10, 2012) and the two 19-μm SO_2 measurements of October 4, 2012, which were taken using different transitions (E12, E13). For the conversion from HDO to H_2O abundances on Venus, we assume a D/H ratio of 200 times the VSMOW (Fedorova et al. 2008).

submillimeter observations (Sandor et al. 2010, 2012; Encrenaz et al. 2015b) and from VEx-SPICAV data (Belyaev et al. 2012; Marcq et al. 2013) that the SO_2 vertical distribution is depleted in the lower mesosphere but increases again with the altitude in the upper mesosphere. In what follows, we keep the assumption of an SO_2 cutoff at 68 km, as inferred from the TEXES data of October 2012, but we keep in mind that, according to the VEX-SPICAV data, this cutoff is located at slightly higher levels. In the absence of cutoff, our results on the SO_2 mixing ratio at the cloudtop would be decreased by a factor of between approximately two and three (Figs. 13–16).

4.3. Long-term variability of SO_2 and HDO

Figure 21 shows the variations of the HDO and SO_2 volume mixing ratio over a period of four years. In the case of SO_2, both datasets, at 7.4 and 19 μm, are shown. For each point, the volume mixing ratios have been inferred (assuming for SO_2 a cutoff at 68 km) from the line depth ratios measured in the integrated spectra, and the error bars have been estimated taking into account the quality of the data. Volume mixing ratios have been derived from the line depth ratios (ldr) using the conversion factors derived from our spectral fits:

1345 cm^{-1} data: $vmr(SO_2)(ppbv) = ldr(SO_2) \times 600.$, $vmr(H_2O)(ppmv) = ldr(HDO) \times 1.5$.

530 cm^{-1} data: $vmr(SO_2)(ppbv) = ldr(SO_2) \times 500$. It can be seen from Fig. 21 that the water content at the cloudtop is remarkably constant between 2012 and 2016, taking into account the error bars. There is one exception, however, corresponding to the March 2015 data that shows, in one case, an H_2O increase by a factor of 1.5 to 2. It is interesting to notice that this point corresponds to an observation taken at the evening terminator, while all other datasets (except January 2012) correspond to morning terminators. One could thus wonder if this excess could be a local temperature effect, as temperatures in the lower mesosphere are expected to be higher in the evening than in the morning (Lebonnois et al. 2010, 2016). However, if this explanation is correct, we would expect to see a day vs. night effect in the HDO maps, which is not the case. Future observations of the evening terminator, in early 2017, should bring more information to this question. It must be noted also that the limb enhancement noticed in January 2012 (E12) has not been observed later.

As mentioned earlier in this paper, at the cloudtop and a few kilometers below, the SO_2 content shows strong variations, by a factor as much as ten. It does not look like a long-term trend, as the SO_2 abundance shows two local maxima, in January 2012 and in January 2016. The correlation between the 7.4-μm data and the 19-μm data is usually good, except in July 2014, where there might be a depletion of the SO_2 content in the few upper kilometers of the upper cloud. More data will be necessary to confirm this effect.

The long-term variability of H_2O and SO_2 in the mesosphere of Venus has been studied using photochemical models and global circulation models (Mills et al. 2007; Zhang et al. 2010, 2012; Parkinson et al. 2015). Photochemical models show that the mesospheric SO_2 content can control the water distribution at high altitude, which might induce an anticorrelation between the two species. Unfortunately, our data are not precise enough to detect water temporal variations at a level lower than 100 ppbv. As mentioned above, taking into account the error bars, the disk-integrated water content at the cloudtop appears globally constant with time.

4.4. Short-term variability of SO_2

It can be seen from Figs. 10 and 12 that the SO_2 features at the cloudtop have a lifetime in the range of a few hours. We note that the 30-min variation in the 19-μm data of October 4, 2012 mentioned in E13 was most likely an artifact. No other effect of this kind has been observed in subsequent datasets, and we have realized that continuum fluctuations within the disk might have been responsible for such an effect.

The existence of localized plumes of SO_2, preferentially emitted at low latitudes (as observed in the TEXES data), could reflect convective activity and possible uplift of SO_2 from deeper layers, as already suggested by Esposito (1988), Marcq et al. (2013) and Lefèvre et al. (2016). The timescale of the SO_2 variability that we observe (about a few hours) is also consistent with the value of 10^5 s derived by Marcq et al. (2013) using SPICAV-UV observations. However, there is still an open question about the lifetime of these plumes, as they appear to be shorter than that predicted by photochemical and dynamical models (Lefèvre et al. 2016). Also, we need to understand why plumes are observed in the case of SO_2, but not H_2O. A possible explanation might be that at the cloudtop, the water content is typically ten times more abundant than sulfur dioxide. Assuming that equal quantities of both molecules are involved in the H_2SO_4 condensation and sublimation cycle, one could expect that the relative variations of H_2O would be in the range of 100 ppbv at most, that is, only 10% or less of its mean value. Such variations might be too small for the sensitivity limit of the TEXES data.

5. Conclusions

In this paper, we have continued our analysis of the mapping of SO_2 and HDO at the cloudtop of Venus by considering six datasets obtained between January 2012 and January 2016. Two datasets have been recorded in which the evening terminator was

observed, while the four others correspond to the morning terminator. We have focussed on the retrieval of the SO_2 and HDO abundances by using weak transitions of these species and by dividing their line depths by the line depth of a neighboring weak CO_2 line. To first order, this method does not request the exact knowledge of the thermal profile. The study of the thermal structure as a function of latitude and time will be done in a forthcoming publication.

The main results of the present study can be summarized as follows:

- The HDO distribution is relatively uniform within the disk and shows limited temporal variations, on both short-term and long-term timescales. Mean disk-integrated H_2O volume mixing ratio (assuming a D/H ratio of 200 × VSMOW in the Venus mesosphere) typically ranges between 1.0 and 1.5 ppmv.
- In contrast, the SO_2 maps show strong variations over the disk, by a factor as much as 5. Short-term variations seem to have a timescale of a few hours. For intervals of about 2 h, the SO_2 features at the cloudtop are often shown to follow the four-day rotation of the clouds. We have no confirmation of short-term (i.e., shorter than an hour) variations of the SO_2 maps at 19 μm as suggested in E13. We believe that these maps have to be considered with caution because of possible fluctuations of the continuum curvature over the map.
- Our data are consistent with a cutoff in the vertical distribution of SO_2, with no SO_2 above a level situated a few kilometers above the cloudtop. The exact altitude of this level depends upon the thermal profile used in our calculations. In addition, our data show little sensitivity to the exact altitude of this level. A higher spectral resolution would help to better constrain this level.
- The TEXES data are consistent with a constant vertical distribution of H_2O. Whereas a cutoff as observed for SO_2 can be excluded in the case of H_2O, the TEXES sensitivity, however, is not sufficient to discriminate between a constant water mixing ratio throughout the mesosphere, and a moderate depletion by a factor of 2 at about z = 85 km, as suggested by photochemical models (Zhang et al. 2012).
- The SO_2 mixing ratios (calculated assuming a cutoff at a constant altitude for all datasets) show a variation by a factor of ten between 2012 and 2016. The minimum value is observed in February 2014 while the maximum value is found in January 2016. We note that, because of our limited spectral resolution, the TEXES data are sensitive to the column density of the minor species rather than their mixing ratio at a given level. Nevertheless, we convert this quantity into a mixing ratio at the cloudtop for an easier comparison with other datasets.

Acknowledgements. T.E., T.K.G., M.J.R. and C.D.W. were visiting astronomers at the InfraRed Telescope Facility, which is operated by the University of Hawaii under Cooperative Agreement no. NNX-08AE38A with the National Aeronautics and Space Administration, Science Mission Doctorate, Planetary Astronomy Program. We thank the IRTF staff for the support of TEXES observations. Observations with TEXES were supported by NSF Grants NNX-14AG-34G for T.K.G. and AST-0708074 for M.J.R. T.K.G. acknowledges support by NASA Grant NNX14AG34G. T.E. and B.B. acknowledge support from CNRS and Programme National de Planétologie (INSU), and T.F. aknowledges support from UPMC. T.W. acknowledges support from the University of Versailles-St-Quentin and the European Commission Framework Program FP7 under Grant Agreement 606798 (Project EuroVenus). T.E. acknowledges support from the Jet Propulsion Laboratory as a Distinguished Visiting Scientist. We are grateful to Emmanuel Marcq for helpful comments regarding the discussion.

References

Belyaev, D. A., Korablev, O., Fedorova, A., et al. 2008, J. Geophys. Res., 113, E00B25
Belyaev, D. A., Montmessin, F., Bertaux, J.-L., et al. 2012, Icarus, 217, 740
Crisp, D. 1986, Icarus, 67, 484
Bertaux, J.-L., Vandaele, A.-C., Korablev, O., et al. 2007, Nature, 450, 646
Encrenaz, T., Bézard, B., Owen, T., Lebonnois, S., et al. 2005, Icarus, 179, 43
Encrenaz, T., Greathouse, T. K., Richter, M. J., et al. 2008, Icarus, 195, 547
Encrenaz, T., Greathouse, T. K., Roe, H., et al. 2012, A&A, 543, A153
Encrenaz, T., Greathouse, T. K., Lefèvre, F., et al. 2015a, A&A, 578, A127
Encrenaz, T., Moreno, R., Moullet, A., et al. 2015b, Plan. Space Sci., 113, 27
Esposito, L. W. 1984, Science, 223, 1072
Fedorova, A., Korablev, O., Vandaele, A.-C., et al. 2008, J. Geophys. Res., 113, E00B25
Gurwell, M. A., Melnick, G. J., Tolls, V., et al. 2007, Icarus, 288, 2007
Jacquinet-Husson, N., Scott, N., Chedin, A., et al. 2008, J. Quant. Spectr. Rad. Transfer, 109, 1043
Krasnopolsky, V. A. 1986, Photochemistry of the atmospheres of Mars and Venus (New York: Springer-Verlag)
Krasnopolsky, V. A. 2010, Icarus, 209, 314
Lacy, J. H., Richter, M. J., Greathouse, T. K., et al. 2002, PASP, 114, 153
Lebonnois, S., Sugimoto, N., & Gilli, G. 2010, J. Geophys. Res., 115, E06006
Lebonnois, S., Sugimoto, N., & Gilli, G. 2016, Communication presented at the Venus International Conference, Oxford, April 2016
Lefèvre, F., Stolzenbach, A., Mattaanen, A., et al. 2016, Communication presented at the International Venus Conference, Oxford, April 2016
Marcq, E., Bertaux, J.-L., Montmessin, F., & Belyaev, D. 2013, Nature Geoscience, 6, 25
Migliorini, A., Grassi, D., Montabone, L., et al. 2012, Icarus, 217, 669
Mills, F. P., Esposito, L. W., & Yung, Y. K. 2007, in Exploring Venus as a Terrestrial Planet, Geophysical Monograph Series, 176, 73
Nakazawa, T., & Tanaka, M. 1982, J. Quant. Spectr. Rad. Transf., 28, 409
Parkinson, C., Gao, P., Esposito, L., et al. 2015, Plan. Space Sci., 113, 226
Pugh, L. A., & Rao, K. N. 1976, Intensities from infrared spectra. In Molecular Spectroscopy, Modern Research, Volume II, Academic Press
Rohlfs, K., & Wilson, T. L. 2004, Tools for radioastronomy, 4th edn. (Berlin: Springer)
Rothman, L. S., Rinsland, C. P., Golman, A., et al. 2005, J. Quant. Spectr. Rad. Transf., 60, 665
Sandor, B. J., Clancy, R. T., Moriartry-Schieven, G., & Mills, F. P. 2010, Icarus, 208, 49
Sandor, B. J., Clancy, R. T., & Moriartry-Schieven, G. 2012, Icarus, 217, 839
Tellmann, S., Paetzold, M., Hausler, B., et al. 2009, J. Geophys. Res., 114, E00B36, DOI: 10.1029/2008JE003204
Vandaele, A.-C., Mahieux, A., Wilquet, V., et al. 2016, Communication presented at the International Venus Conference, Oxford, April 2016
Varanasi, P. 1971, J. Quant. Spectr. Rad. Transf., 11, 223
Yamamoto, M., & Takahashi, M. 2012, Icarus, 217, 714
Zasova, L. V., Moroz, V. I., Esposito, E. W., & Na, C. Y. 1993, Icarus, 105, 92
Zhang, X., Liang, M. C., Montmessin, F., et al. 2010, Nature Geosci. Lett., 3, 834
Zhang, X., Liang, M. C., Mills, F. P., et al. 2012, Icarus, 217, 714